Influence of Bi on the thermoelectric properties of SrTiO3-δ

Cong Chen, Mohamed Ali Bousnina, Fabien Giovannelli, Fabian Delorme

Influence of Bi on the thermoelectric properties of $SrTiO_{3-\delta}$

Cong Chen[1,2], Mohamed Bousnina[1], Fabien Giovannelli[1], and Fabian Delorme[1]

[1] Université de Tours, CNRS, INSA CVL, GREMAN UMR 7347, IUT de Blois, 15 rue de la chocolaterie, CS 2903, 41029 Blois Cedex, France

[2] Bundesanstalt für Materialforschung und –prüfung (BAM), Unter den Eichen 87, 12205 Berlin, Germany

Corresponding author: Cong Chen. E-mail: saracongchen@gmail.com

Abstract

The thermoelectric properties of $Sr_{1-x}Bi_xTiO_{3-\delta}$ ($0 \leq x \leq 0.07$) have been investigated. Dense ceramics of $Sr_{1-x}Bi_xTiO_{3-\delta}$ and $Sr_{0.95}TiO_{3-\delta}$ have been prepared by solid-state reaction and conventional sintering in air followed by annealing in a reducing atmosphere. XRD and SEM analyses show that the rutile TiO_2 in $Sr_{0.95}TiO_3$ formed after sintering becomes Magnéli phase of Ti_nO_{2n-1} after annealing. Moreover, Bi resolves from $Sr_{1-x}Bi_xTiO_3$ after annealing, resulting in the formation of $Sr_{1-x}Bi_xTiO_{3-\delta}/Bi/Ti_nO_{2n-1}$ composites. With increasing Bi content in $Sr_{1-x}Bi_xTiO_{3-\delta}$, the electrical conductivity increases while the absolute values of the Seebeck coefficient decrease as a result of increasing carrier concentration. The thermal conductivity of $SrTiO_{3-\delta}$ is reduced by doping Bi up to $x = 0.07$. Highest $ZT \sim 0.13$ is obtained in $Sr_{0.93}Bi_{0.07}TiO_{3-\delta}$ at 1000 K.

Keywords: thermoelectrics; $SrTiO_3$; composite; Bi; Magnéli phase

1. Introduction

Oxide thermoelectric materials have the advantages of low cost, low toxicity, and good chemical stability at high temperatures. High-performance p-type thermoelectric oxides include layered cobalt oxides containing 2D edge sharing CoO_6 octahedra [1-6] and acceptor-doped perovskite $LaCoO_3$ [7-10], while n-type oxides include donor-doped $SrTiO_3$ [11-13], $CaMnO_3$ [14], Al-doped ZnO [15, 16], etc. Among them, donor-doped $SrTiO_3$ exhibits a large Seebeck coefficient due to a large carrier effective mass and the orbital degeneracy of Ti 3d-t_{2g} conduction band [11]. Its electrical conductivity can be tuned from insulating to metallic through substitutional doping and/or introducing oxygen deficiency. Usually, $SrTiO_3$ is sintered under a reducing atmosphere and doped with rare-earth elements on Sr^{2+} sites and/or Nb^{5+} on Ti^{4+} sites [17-19]. By adjusting dopants and doping concentration, the electrical conductivity can be improved due to increased carrier concentration, while the lattice thermal conductivity can be reduced by strain field scattering, mass fluctuation and point defects [20, 21].

High figure of merit (ZT) values in the range of 0.30 – 0.41 have been reported in $SrTiO_3$ substituted by 8% La and 12% Dy (double substitution) [22], 10% Pr with A-site deficiency [23], 10% Y [24],

10% – 15% Nb [25], 15% La and A-site vacancies [26], etc. Moreover, similar high *ZT* values have been achieved in composites consisting of La/Nb doped $SrTiO_3$ and Cu/Fe [27]. However, the *ZT* values of doped $SrTiO_3$ are still low compared to traditional thermoelectric materials owing to its high lattice thermal conductivity. Therefore, nanostructuring approaches have been adopted to enhance the phonon scattering, such as synthesizing $SrTiO_3$ nanoparticles [28], introducing nanoinclusions [29, 30], and fabricating $SrTiO_3$ superlattices [31], etc. Moreover, Ruddlesden-Popper (RP) phases of $SrO(SrTiO_3)_n$ with a layered crystal structure have been investigated [32, 33]. Although a decrease in the thermal conductivity is achieved in the RP phases, the electrical conductivity also decreases due to the insulating SrO layers, resulting in lower values of *ZT* than donor-doped $SrTiO_3$.

In this work, we aim to investigate the effect of Bi^{3+} substitution on the thermoelectric properties of $SrTiO_{3-\delta}$. By replacing Sr^{2+} with Bi^{3+}, we intend to i) improve the electrical conductivity by increased carrier concentration, and ii) reduce the lattice thermal conductivity due to the large mass difference between Bi^{3+} and Sr^{2+}. Gong et al. reported that a *ZT* value of 0.269 at 1073 K can be achieved in La- and Bi-codoped $SrTiO_3$ [34]. However, it is not clear whether the improved thermoelectric properties are due to La or Bi. Therefore, it is necessary to study $SrTiO_3$ with a single type of dopant, Bi. This paper reports the thermoelectric properties of $Sr_{1-x}Bi_xTiO_{3-\delta}$ ($0 \leq x \leq 0.07$) and $Sr_{0.95}TiO_{3-\delta}$ in the temperature range of 300 K – 1000 K, synthesized by solid-state reaction and conventional sintering.

2. Experiment

Powders of $Sr_{1-x}Bi_xTiO_3$ (x = 0, 0.005, 0.01, 0.03, 0.05, and 0.07) and $Sr_{0.95}TiO_3$ were synthesized by solid state reaction. Stoichiometric amounts of $SrCO_3$ (Sigma Aldrich, ≥ 98%), Bi_2O_3 (Acros Organics, ≥ 99.9%), and TiO_2 (Sigma Aldrich, ≥ 99.9%) powders were mixed by planetary ball mill (RETSCH PM100) at 250 rpm for 5 min with a tungsten carbide jar and beads. The powder mixture was pelletized by a uniaxial pressing machine and calcined at 1373 K for 2 h over ZrO_2 beads in an alumina crucible in air. The pellets were ball milled again at 250 rpm for 5 min. The powder was pressed into pellets and sintered at 1673 K for 2 h over ZrO_2 beads in an alumina crucible in air, followed by annealing at 1673 K for 12 h in a reducing atmosphere ($67\%N_2/30\%Ar/3\%H_2$).

Room-temperature X-ray diffraction (XRD) was performed by a BRUKER D8 Advance θ/2θ diffractometer equipped with a Linxeye energy-dispersive one-dimensional detector, with Cu-Kα radiation and operating at 40 kV and 40 mA. Scans were recorded from 20° to 85° (2θ) with a step of 0.02° and a counting time of 0.5 s per step. Rietveld refinement was carried out using Fullprof Suite [35]. Microstructure was examined by scanning electron microscopy (SEM, Tescan MIRA3) coupled with a backscattered electron detector (BSD) and an energy-dispersive X-ray spectroscopy (EDS, Oxford INCA X-act). Samples were gold-coated by sputtering prior to observation.

Electrical conductivity and Seebeck coefficient were measured simultaneously by ULVAC ZEM3 in a low pressure He atmosphere from a high of 1000 K to a low of 323 K. Points of contact between

samples and two thermocouples were coated with a thin layer of gold to reduce the contact resistance. Thermal conductivity is a product of density, thermal diffusivity, and specific heat capacity. Bulk density was determined from the dry mass and the geometric dimensions of pellets. Graphite coating was applied on the samples for thermal diffusivity measurement (Netzsch LFA457). It was performed from 373 K to 1000 K in vacuum and the data were average values of three measurements at each temperature. Specific heat capacity was measured from room temperature up to 1000 K, with a heating rate of 20 K.min^{-1} in platinum crucibles in a nitrogen atmosphere (NETZSCH STA449 F3).

3. Results and discussion

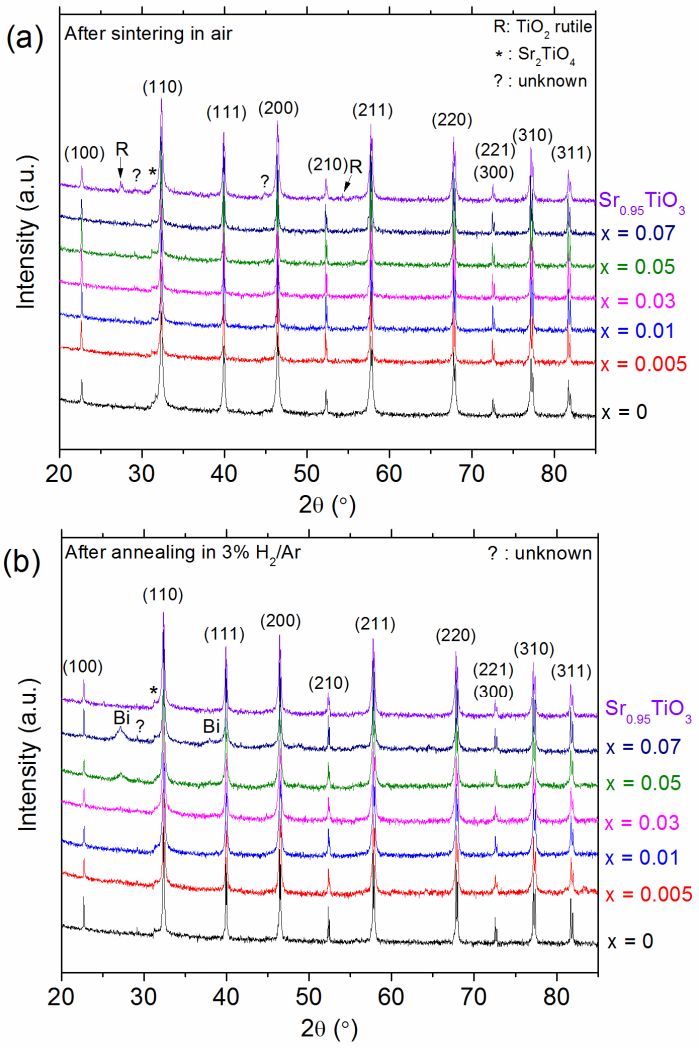

Fig. 1 X-ray diffraction patterns of $Sr_{1-x}Bi_xTiO_{3-\delta}$ (x = 0, 0.005, 0.01, 0.03, 0.05, and 0.07) and $Sr_{0.95}TiO_{3-\delta}$ ceramics (a) after sintering in air and (b) after annealing in a reducing atmosphere. Letter R, star (*), question mark (?), and Bi indicate diffraction peaks corresponding to rutile TiO_2, Sr_2TiO_4, unknown phases and Bi metal, respectively.

Fig. 1a shows that $Sr_{1-x}Bi_xTiO_3$ ($0 \leq x \leq 0.07$) ceramics exhibit cubic $SrTiO_3$ phase (PDF 00-035-0734) with a space group *Pm-3m* after sintering in air. The intensity is plotted in a logarithmic scale to emphasize the impurity peaks. $Sr_{0.95}TiO_3$ contains an additional rutile TiO_2 phase (PDF 00-021-1276). A satellite peak next to the (110) peak has been observed in every composition, probably corresponding to Sr_2TiO_4, which may appear as an impurity phase during synthesis of $SrTiO_3$ [36]. It is noticed that some samples show a minor diffraction peak at ~ 28º and that $Sr_{0.95}TiO_3$ after sintering in air shows one at ~ 44º. However, it is difficult to determine the phases correctly due to their low intensities and limited number of peaks present. After annealing in a reducing atmosphere (Fig. 1b), diffraction peaks corresponding to Bi metal (PDF 01-079-6675) appear at 2θ of 27.19° and 37.99° in $Sr_{1-x}Bi_xTiO_{3-\delta}$ with x = 0.05 and 0.07 and their diffraction intensity increases with increasing x. Bi metal does not seem to exist in the compositions with lower Bi content. It means that the solubility (or substitution) limit of Bi in $SrTiO_3$ is lower than 5 at. %, or that we are below the XRD detection threshold. Moreover, the diffraction peaks corresponding to rutile TiO_2 can no longer be observed in the XRD pattern of $Sr_{0.95}TiO_{3-\delta}$. All ceramics show densities over 93% of the theoretical density of $SrTiO_3$ calculated from the Rietveld refinements, which are dense enough for the measurement of thermoelectric properties.

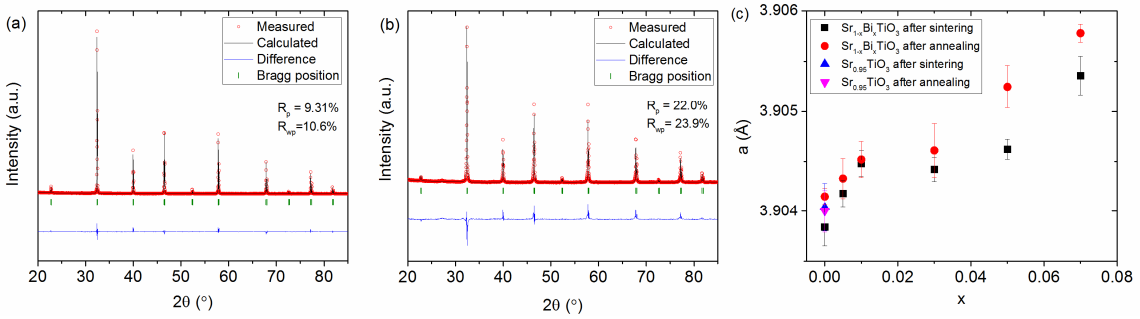

Fig. 2 Examples of Rietveld refinement of $Sr_{1-x}Bi_xTiO_{3-\delta}$ ceramics after annealing in a reducing atmosphere with a composition (a) x = 0 and (b) x = 0.05. (c) Lattice parameter a of $Sr_{1-x}Bi_xTiO_{3-\delta}$ (x = 0, 0.005, 0.01, 0.03, 0.05, and 0.07) and $Sr_{0.95}TiO_{3-\delta}$ after sintering in air and after annealing in a reducing atmosphere versus x.

The XRD patterns as shown in Fig. 1 are refined to calculate lattice parameters. Fig. 2a and b show two examples of the refined XRD patterns of $Sr_{1-x}Bi_xTiO_{3-\delta}$ with x = 0 and 0.05 after annealing in a reducing atmosphere. The poor Rietveld refinement in Fig. 2b is probably due to the presence of the above-mentioned impurities. The lattice parameter a of the air-sintered and reducing atmosphere-annealed samples is shown in Fig. 2c. In both cases, the lattice parameter of $Sr_{1-x}Bi_xTiO_{3-\delta}$ increases with increasing Bi content, although the ionic radius of Sr^{2+} (1.26 Å) is larger than that of Bi^{3+} (1.17 Å) [37]. As the ionic radius for Bi^{3+} in twelve-fold coordination is not available, the ionic radii in eight-fold coordination for both ions are used here. The unit cell expansion could be attributed to the

formation of oxygen vacancies and Ti^{3+} ions. Oxygen vacancy induces an increase in the Coulomb repulsion between neighboring transition metals ions, thus increasing unit cell volume. Moreover, the extra charge induced by Bi^{3+} substitution and oxygen vacancies could be compensated by partial reduction of Ti^{4+} (0.605 Å) into Ti^{3+} (0.67 Å) [37]. The lattice parameters of the reducing atmosphere-annealed samples are larger than those of the air-sintered samples at each Bi content, which is most probably due to increased oxygen deficiency. The lattice parameters of air-sintered and reducing atmosphere-annealed $Sr_{0.95}TiO_3$ are similar to the undoped $SrTiO_3$ and less than the Bi-doped samples, indicating the existence of Bi dopant in the crystal structure of $Sr_{1-x}Bi_xTiO_{3-\delta}$ in spite of the appearance of Bi metal.

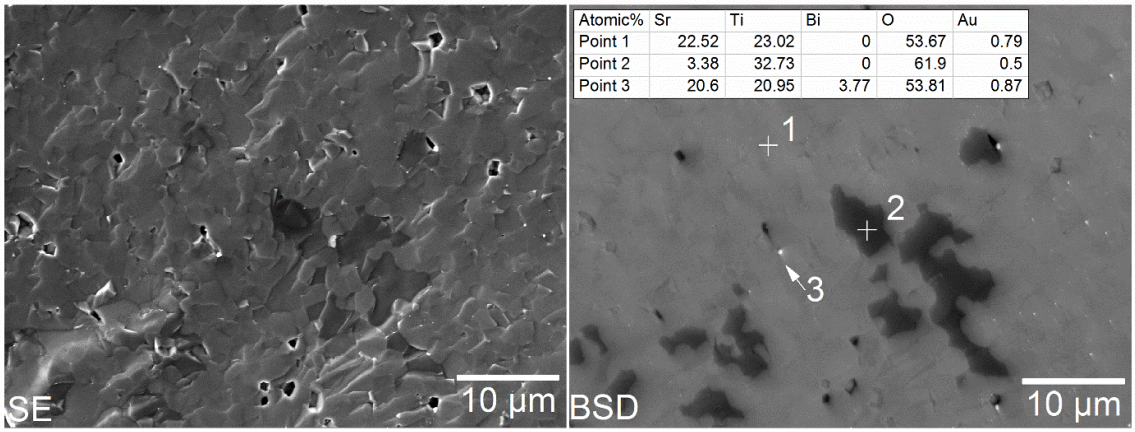

Fig. 3 SEM and BSD images of fracture surface of $Sr_{1-x}Bi_xTiO_{3-\delta}$ with x = 0.01 after annealing in a reducing atmosphere. The insert in the BSD image shows the atomic ratio of elements at three indicated points measured by EDS.

Fig. 3 shows SEM and BSD images of a fracture surface of the annealed $Sr_{1-x}Bi_xTiO_{3-\delta}$ ceramic with x = 0.01. XRD only shows the existence of Bi metal in the composition with x = 0.05 and 0.07. It is not known whether the absence of diffraction peaks corresponding to Bi metal in $Sr_{1-x}Bi_xTiO_{3-\delta}$ with x < 0.05 is due to that it is below the solubility of Bi or detection limit of the XRD instrument. Therefore, the microstructure of the composition with x = 0.01 was examined. The BSD image shows a clear contrast between different phases. The atomic ratio between different elements from EDS analysis is shown in the insert of Fig. 3. The light grey area shows a similar atomic ratio between Sr and Ti, indicating that it is most likely $SrTiO_3$. The bright spots are rich in Bi, while the liquid-like dark areas are rich in Ti. Therefore, Bi metal exists in $Sr_{1-x}Bi_xTiO_{3-\delta}$ even at a Bi content lower than what has been indicated in the XRD analysis (Fig. 1b). It is ascribed to the decomposition of $Sr_{1-x}Bi_xTiO_{3-\delta}$ after annealing at 1673 K under a reducing atmosphere, in agreement with a previous study on the degradation of $SrBi_2Ta_2O_9$ in which $SrBi_2Ta_2O_9$ decomposes into Bi metal and Sr-Ta oxide above 573 K under 4%H_2/Ar atmosphere [38]. Bi metal and Ti-rich phase have also been observed in $Sr_{1-x}Bi_xTiO_{3-\delta}$ ceramics with other Bi contents. The Ti-rich phase is Magnéli phase (Ti_nO_{2n-1}), a commonly

found phase in Sr deficient $SrTiO_3$ [39]. As Bi leaves the lattice site, $Sr_{1-x}Bi_xTiO_{3-\delta}$ becomes A-site deficient and Ti_nO_{2n-1} is formed. Ti_nO_{2n-1} is also observed in $Sr_{0.95}TiO_{3-\delta}$ as a result of excess TiO_2. It is believed that above the solubility limit of Sr vacancy in the $SrTiO_3$ structure, Ti_nO_{2n-1} will form as a secondary phase in a reducing atmosphere.

Fig. 4a and b show the temperature dependence of the electrical conductivity and Seebeck coefficient of $Sr_{1-x}Bi_xTiO_{3-\delta}$ and $Sr_{0.95}TiO_{3-\delta}$. $Sr_{1-x}Bi_xTiO_{3-\delta}$ with $0 \leq x \leq 0.005$ shows semiconducting electrical conductivity over the whole range of temperature, while the samples with $0.01 \leq x \leq 0.07$ show metallic conduction above 400 K. The electrical conductivity of $Sr_{1-x}Bi_xTiO_{3-\delta}$ increases with increasing Bi content up to $x = 0.05$. All compositions are n-type, as they possess negative values of Seebeck coefficient. In general, the absolute values of Seebeck coefficient decrease with increasing Bi until $x = 0.05$. An increase in the carrier concentration via Bi substitution is confirmed by the simultaneous increase in electrical conductivity and decrease in the absolute values of Seebeck coefficient. $Sr_{0.95}TiO_{3-\delta}$ has been synthesized to confirm the role of Bi substitution and Ti_nO_{2n-1} in $SrTiO_{3-\delta}$. Compared to $SrTiO_{3-\delta}$, $Sr_{0.95}TiO_{3-\delta}$ possesses higher electrical conductivity and lower absolute values of Seebeck coefficient, possibly due to the presence of Ti_nO_{2n-1} in $Sr_{0.95}TiO_{3-\delta}$. Ti_nO_{2n-1} is a series of n-type thermoelectric materials and possesses better thermoelectric performance than the undoped $SrTiO_{3-\delta}$ in this work [40, 41]. Therefore, the incorporation of Ti_nO_{2n-1} in $SrTiO_{3-\delta}$ could improve its electrical conductivity and reduce its absolute values of Seebeck coefficient. On the other hand, $Sr_{0.95}TiO_{3-\delta}$ shows a much lower electrical conductivity than $Sr_{0.95}Bi_{0.05}TiO_{3-\delta}$. It could be due to its low carrier concentration and probably low mobility. It is clear from Fig. 2c that the lattice parameter of $Sr_{0.95}TiO_{3-\delta}$ is similar to the undoped $SrTiO_{3-\delta}$ and smaller than all of the Bi-doped samples, indicating a lack in the carrier concentration contributed by Bi substitution and oxygen deficiency. Moreover, below a critical carrier concentration, the carrier mobility of $SrTiO_{3-\delta}$ decreases with decreasing carrier concentration [42]. Finally, the Seebeck coefficient of the samples presents a very complex behaviour, with abrupt variations without any observable counterparts in the electrical conductivity measurements, except for the sample with x = 0.03 at T ~ 700 K. Ohta et al. [17] have shown that such transition at 750 K in heavily La-and Nb-substituted $SrTiO_3$ samples can be related to a dominant carrier scattering mechanism changing with increasing temperature from a coupled scattering by polar optical phonons and acoustic phonons to mere acoustic phonon scattering. Moreover, the samples in this study are composites with complex microstructures rather than single crystals as in Ohta's et al. study, which could be related to these variations. However, further studies (such as Hall effect measurements, magnetic measurements …) are required to understand such complex behaviour. Power factor (Fig. 4c) can be calculated from electrical conductivity and Seebeck coefficient. The power factor of $SrTiO_{3-\delta}$ is significantly improved by Bi substitution, especially at temperatures ~ 400 K. The highest power factor is obtained in $Sr_{1-x}Bi_xTiO_{3-\delta}$ with $x = 0.07$, ~ 1286

$\mu Wm^{-1}K^{-2}$ at 420 K, which is comparable with that of La and Y-doped $SrTiO_3$ at a similar doping concentration [21, 43].

Fig. 4d shows that 0.5% of Bi substitution does not obviously reduce the thermal conductivity of $SrTiO_3$, whereas 5% and 7% of Bi doped $SrTiO_{3-\delta}$ and $Sr_{0.95}TiO_{3-\delta}$ exhibit reduced thermal conductivity. The reduction of the thermal conductivity in $Sr_{1-x}Bi_xTiO_{3-\delta}$ with x = 0.05 and 0.07 could be attributed to Bi substitution and the composite effect from Bi metal and Ti_nO_{2n-1}. The mass difference between Sr^{2+} and Bi^{3+} creates point defect scattering for phonons, thus reducing the lattice thermal conductivity. The interfaces between different phases could scatter phonons, especially the interfaces between Bi metal and the two oxides. Lyeo and Cahill have observed a low thermal conductance at the interfaces between Bi and hydrogen-terminated diamond, with a thermal conductivity approaching amorphous limit [44]. They ascribe it to the dissimilar Debye temperatures and vibrational spectra between Bi and diamond. As the Debye temperature of Bi [44] is much lower than those of $SrTiO_3$ [45] and TiO_2 [46], a low thermal conductivity could be expected at the interfaces between Bi and oxides. Moreover, the shear planes in Ti_nO_{2n-1} can also effectively scatter phonons.

Fig. 4e shows the temperature dependence of figure of merit. *ZT* of $Sr_{1-x}Bi_xTiO_{3-\delta}$ is enhanced by substituting Sr with Bi up to x = 0.07, reaching ~ 0.13 at 1000 K. In addition, *ZT* of $Sr_{0.95}TiO_{3-\delta}$ is a little higher than that the undoped $SrTiO_3$ but much lower than that of $Sr_{0.95}Bi_{0.05}TiO_{3-\delta}$. Incorporating Bi into $SrTiO_{3-\delta}$ is beneficial for its high power factor and low thermal conductivity due to the substitution and metal inclusion, whereas a further enhancement of *ZT* in Bi-doped $SrTiO_3$ is limited by its low solubility. Therefore, Bi can be added as a co-dopant into $SrTiO_{3-\delta}$.

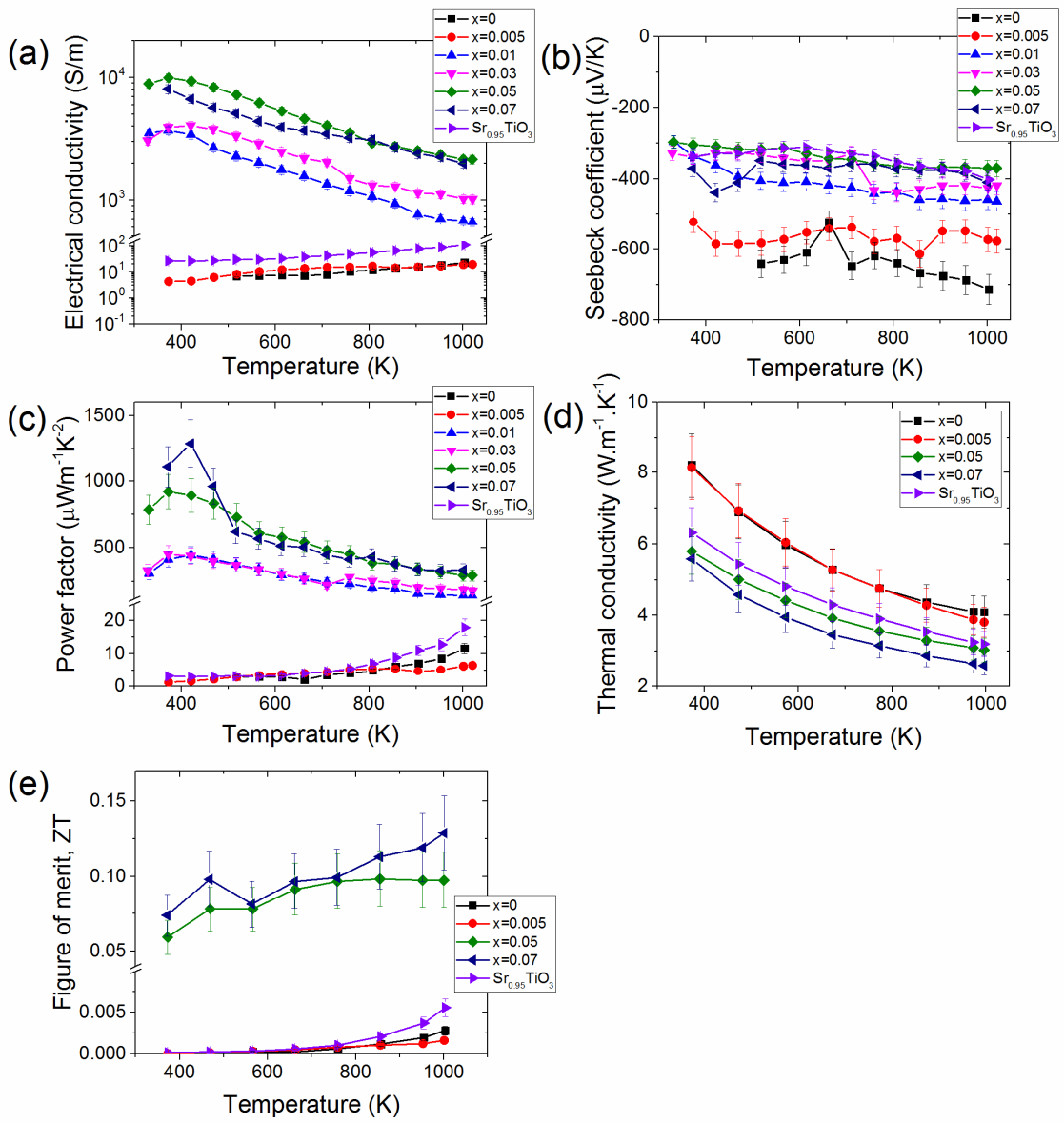

Fig. 4 Thermoelectric properties of $Sr_{1-x}Bi_xTiO_{3-\delta}$ (x = 0.005, 0.01, 0.03, 0.05, and 0.07) and $Sr_{0.95}TiO_{3-\delta}$ ceramics after annealing in a reducing atmosphere as a function of temperature. (a) Electrical conductivity, (b) Seebeck coefficient, (c) power factor, (d) thermal conductivity, and (e) figure of merit, *ZT*.

4. Conclusions

The thermoelectric properties of dense $Sr_{1-x}Bi_xTiO_{3-\delta}$ ($0 \leq x \leq 0.07$) and $Sr_{0.95}TiO_{3-\delta}$ ceramics prepared by solid-state reaction and conventional sintering have been studied. The presence of Bi metal and Ti_nO_{2n-1} has been confirmed in $Sr_{1-x}Bi_xTiO_{3-\delta}$ ceramics, making them $Sr_{1-x}Bi_xTiO_{3-\delta}$/Bi/$Ti_nO_{2n-1}$ composites. Ti_nO_{2n-1} is also observed in $Sr_{0.95}TiO_3$. The lattice parameter of $Sr_{1-x}Bi_xTiO_{3-\delta}$ increases with increasing Bi content, whereas undoped $SrTiO_{3-\delta}$ possesses the same lattice parameter as

$Sr_{0.95}TiO_{3-\delta}$. It indicates that some Bi dopants are incorporated into the crystal lattice of $SrTiO_3$. Substitution of Sr^{2+} with Bi^{3+} increases the electrical conductivity and reduces the absolute values of Seebeck coefficient. The power factor is improved in the Bi-doped samples. The thermal conductivity is effectively reduced in $Sr_{1-x}Bi_xTiO_{3-\delta}$ with x = 0.05 and 0.07, possibly due to the enhanced phonon scattering introduced by Bi substitution and the composite effect from Bi and Ti_nO_{2n-1}. Highest ZT ~ 0.13 has been achieved in $Sr_{0.93}Bi_{0.07}TiO_{3-\delta}$ at 1000 K.

Conflict of interest

Authors declare that there are no conflicts of interest.

References

1. Terasaki, I., Y. Sasago, and K. Uchinokura, *Large thermoelectric power in $NaCo_2O_4$ single crystals.* Phys. Rev. B, 1997. **56**(20): p. R12685-R12687.
2. Masset, A.C., C. Michel, A. Maignan, M. Hervieu, O. Toulemonde, F. Studer, B. Raveau, and J. Hejtmanek, *Misfit-layered cobaltite with an anisotropic giant magnetoresistance: $Ca_3Co_4O_9$.* Physical Review B, 2000. **62**(1): p. 166-175.
3. Shikano, M. and R. Funahashi, *Electrical and thermal properties of single-crystalline $(Ca_2CoO_3)_{0.7}CoO_2$ with a $Ca_3Co_4O_9$ structure.* Applied Physics Letters, 2003. **82**(12): p. 1851-1853.
4. Delorme, F., C.F. Martin, P. Marudhachalam, D. Ovono Ovono, and G. Guzman, *Effect of Ca substitution by Sr on the thermoelectric properties of $Ca_3Co_4O_9$ ceramics.* Journal of Alloys and Compounds, 2011. **509**(5): p. 2311-2315.
5. Chen, C., T. Zhang, R. Donelson, D. Chu, R. Tian, T.T. Tan, and S. Li, *Thermopower and chemical stability of $Na_{0.77}CoO_2/Ca_3Co_4O_9$ composites.* Acta Mater., 2014. **63**: p. 99-106.
6. Delorme, F., C. Chen, B. Pignon, F. Schoenstein, L. Perriere, and F. Giovannelli, *Promising high temperature thermoelectric properties of dense $Ba_2Co_9O_{14}$ ceramics.* J. Eur. Ceram. Soc., 2017. **37**(7): p. 2615-2620.
7. Androulakis, J., P. Migiakis, and J. Giapintzakis, *$La_{0.95}Sr_{0.05}CoO_3$: An efficient room-temperature thermoelectric oxide.* Appl. Phys. Lett., 2004. **84**(7): p. 1099-1101.
8. Kozuka, H., K. Yamagiwa, K. Ohbayashi, and K. Koumoto, *Origin of high electrical conductivity in alkaline-earth doped $LaCoO_3$.* J. Mater. Chem., 2012. **22**(22): p. 11003-11005.
9. Chen, C., F. Giovannelli, T. Chartier, and F. Delorme, *Synthesis and thermoelectric properties of doubly substituted $La_{0.95}Sr_{0.05}Co_{1-x}Cr_xO_3$ ($0 \leqslant x \leqslant 0.5$).* Mater. Res. Bull., 2018. **102**: p. 257-261.
10. Bousnina, M.A., R. Dujardin, L. Perriere, F. Giovannelli, G. Guegan, and F. Delorme, *Synthesis, sintering, and thermoelectric properties of the solid solution $La_{1-x}Sr_xCoO_{3\pm\delta}$ ($0 \leqslant x \leqslant 1$).* Journal of Advanced Ceramics, 2018. **7**(2): p. 160-168.
11. Okuda, T., K. Nakanishi, S. Miyasaka, and Y. Tokura, *Large thermoelectric response of metallic perovskites: $Sr_{1-x}La_xTiO_3$ ($0 \leqslant x \leqslant 0.1$).* Phys. Rev. B, 2001. **63**(11): p. 113104.
12. Chen, C., T. Zhang, R. Donelson, T.T. Tan, and S. Li, *Effects of yttrium substitution and oxygen deficiency on the crystal phase, microstructure, and thermoelectric properties of $Sr_{1-1.5x}Y_xTiO_{3-\delta}$ ($0 \leqslant x \leqslant 0.15$).* J. Alloys Compd., 2015. **629**: p. 49-54.
13. Kovalevsky, A.V., M.H. Aguirre, S. Populoh, S.G. Patrício, N.M. Ferreira, S.M. Mikhalev, D.P. Fagg, A. Weidenkaff, and J.R. Frade, *Designing strontium titanate-based thermoelectrics: insight into defect chemistry mechanisms.* Journal of Materials Chemistry A, 2017. **5**(8): p. 3909-3922.
14. Flahaut, D., T. Mihara, R. Funahashi, N. Nabeshima, K. Lee, H. Ohta, and K. Koumoto, *Thermoelectrical properties of A-site substituted $Ca_{1-x}Re_xMnO_3$ system.* J. Appl. Phys., 2006. **100**(8): p. 4.

15. Ohtaki, M., T. Tsubota, K. Eguchi, and H. Arai, *High-temperature thermoelectric properties of $(Zn_{1-x}Al_x)O$.* Journal of Applied Physics, 1996. **79**(3): p. 1816-1818.
16. Giovannelli, F., C. Chen, P. Díaz-Chao, E. Guilmeau, and F. Delorme, *Thermal conductivity and stability of Al-doped ZnO nanostructured ceramics.* J. Eur. Ceram. Soc., 2018. **38**(15): p. 5015-5020.
17. Ohta, S., T. Nomura, H. Ohta, and K. Koumoto, *High-temperature carrier transport and thermoelectric properties of heavily La- or Nb-doped $SrTiO_3$ single crystals.* J. Appl. Phys., 2005. **97**(3): p. 034106.
18. Zhang, L., T. Tosh, N. Okinaka, and T. Akiyama, *Thermoelectric properties of combustion synthesized and spark plasma sintered $Sr_{1-x}R_xTiO_3$ (R = Y, La, Sm, Gd, Dy, 0 < x <= 0.1).* Materials Transactions, 2007. **48**(8): p. 2088-2093.
19. Liu, J., C.L. Wang, Y. Li, W.B. Su, Y.H. Zhu, J.C. Li, and L.M. Mei, *Influence of rare earth doping on thermoelectric properties of $SrTiO_3$ ceramics.* J. Appl. Phys., 2013. **114**(22).
20. Dehkordi, A.M., S. Bhattacharya, J. He, H.N. Alshareef, and T.M. Tritt, *Significant enhancement in thermoelectric properties of polycrystalline Pr-doped $SrTiO_3$-delta ceramics originating from nonuniform distribution of Pr dopants.* Applied Physics Letters, 2014. **104**(19).
21. Chen, C., T. Zhang, R. Donelson, T.T. Tan, and S. Li, *Effects of yttrium substitution and oxygen deficiency on the crystal phase, microstructure, and thermoelectric properties of $Sr_{1-1.5x}Y_xTiO_{3-\delta}$ ($0 \leqslant x \leqslant 0.15$).* J. Alloys Compd., 2015. **629**: p. 49-54.
22. Wang, H.C., C.L. Wang, W.B. Su, J. Liu, Y. Sun, H. Peng, and L.M. Mei, *Doping Effect of La and Dy on the Thermoelectric Properties of SrTiO3.* J. Am. Ceram. Soc., 2011. **94**(3): p. 838-842.
23. Kovalevsky, A.V., A.A. Yaremchenko, S. Populoh, A. Weidenkaff, and J.R. Frade, *Effect of A-Site Cation Deficiency on the Thermoelectric Performance of Donor-Substituted Strontium Titanate.* Journal of Physical Chemistry C, 2014. **118**(9): p. 4596-4606.
24. Bhattacharya, S., A.M. Dehkordi, S. Tennakoon, R. Adebisi, J.R. Gladden, T. Darroudi, H.N. Alshareef, and T.M. Tritt, *Role of phonon scattering by elastic strain field in thermoelectric $Sr_{1-x}Y_xTiO_{3-delta}$.* J. Appl. Phys., 2014. **115**(22).
25. Zhang, B., J. Wang, T. Zou, S. Zhang, X. Yaer, N. Ding, C. Liu, L. Miao, Y. Li, and Y. Wu, *High thermoelectric performance of Nb-doped $SrTiO_3$ bulk materials with different doping levels.* Journal of Materials Chemistry C, 2015. **3**(43): p. 11406-11411.
26. Lu, Z., H. Zhang, W. Lei, D.C. Sinclair, and I.M. Reaney, *High-Figure-of-Merit Thermoelectric La-Doped A-Site-Deficient $SrTiO_3$ Ceramics.* Chemistry of Materials, 2016. **28**(3): p. 925-935.
27. Srivastava, D., C. Norman, F. Azough, M.C. Schäfer, E. Guilmeau, and R. Freer, *Improving the thermoelectric properties of $SrTiO_3$-based ceramics with metallic inclusions.* J. Alloys Compd., 2018. **731**: p. 723-730.
28. Park, K., J.S. Son, S.I. Woo, K. Shin, M.-W. Oh, S.-D. Park, and T. Hyeon, *Colloidal synthesis and thermoelectric properties of La-doped $SrTiO_3$ nanoparticles.* Journal of Materials Chemistry A, 2014. **2**(12): p. 4217-4224.
29. Wang, N., H. Chen, H. He, W. Norimatsu, M. Kusunoki, and K. Koumoto, *Enhanced thermoelectric performance of Nb-doped $SrTiO_3$ by nano-inclusion with low thermal conductivity.* Sci. Rep., 2013. **3**.
30. Wang, J., B.-Y. Zhang, H.-J. Kang, Y. Li, X. Yaer, J.-F. Li, Q. Tan, S. Zhang, G.-H. Fan, C.-Y. Liu, L. Miao, D. Nan, T.-M. Wang, and L.-D. Zhao, *Record high thermoelectric performance in bulk $SrTiO_3$ via nano-scale modulation doping.* Nano Energy, 2017. **35**: p. 387-395.
31. Ohta, H., S. Kim, Y. Mune, T. Mizoguchi, K. Nomura, S. Ohta, T. Nomura, Y. Nakanishi, Y. Ikuhara, and M. Hirano, *Giant thermoelectric Seebeck coefficient of a two-dimensional electron gas in $SrTiO_3$.* Nature Materials, 2007. **6**(2): p. 129-134.
32. Lee, K.H., S.W. Kim, H. Ohta, and K. Koumoto, *Ruddlesden-Popper phases as thermoelectric oxides: Nb-doped $SrO(SrTiO_3)_n$ (n= 1, 2).* J. Appl. Phys., 2006. **100**(6): p. 063717.

33. Wang, Y., C. Wan, X. Zhang, L. Shen, K. Koumoto, A. Gupta, and N. Bao, *Influence of excess SrO on the thermoelectric properties of heavily doped $SrTiO_3$ ceramics.* Applied Physics Letters, 2013. **102**(18): p. 183905.
34. Gong, C., G. Dong, J. Hu, Y. Chen, M. Qin, S. Yang, and F. Gao, *Effect of reducing annealing on the microstructure and thermoelectric properties of La–Bi co-doped SrTiO3 ceramics.* Journal of Materials Science: Materials in Electronics, 2017. **28**(19): p. 14893-14900.
35. Rodríguez-Carvajal, J., *Recent developments of the program FULLPROF.* Commission on powder diffraction (IUCr). Newsletter, 2001. **26**: p. 12-19.
36. Boston, R., W.L. Schmidt, G.D. Lewin, A.C. Iyasara, Z. Lu, H. Zhang, D.C. Sinclair, and I.M. Reaney, *Protocols for the Fabrication, Characterization, and Optimization of n-Type Thermoelectric Ceramic Oxides.* Chem. Mater., 2017. **29**(1): p. 265-280.
37. Shannon, R., *Revised effective ionic radii and systematic studies of interatomic distances in halides and chalcogenides.* Acta Crystallogr., Sect. A, 1976. **32**(5): p. 751-767.
38. Shimakawa, Y. and Y. Kubo, *Degradation of ferroelectric $SrBi_2Ta_2O_9$ materials under reducing conditions and their reaction with Pt electrodes.* Applied Physics Letters, 1999. **75**(18): p. 2839-2841.
39. Blennow, P., K.K. Hansen, L. Reine Wallenberg, and M. Mogensen, *Effects of Sr/Ti-ratio in $SrTiO_3$-based SOFC anodes investigated by the use of cone-shaped electrodes.* Electrochimica Acta, 2006. **52**(4): p. 1651-1661.
40. Harada, S., K. Tanaka, and H. Inui, *Thermoelectric properties and crystallographic shear structures in titanium oxides of the Magnèli phases.* Journal of Applied Physics, 2010. **108**(8): p. 083703.
41. Portehault, D., V. Maneeratana, C. Candolfi, N. Oeschler, I. Veremchuk, Y. Grin, C. Sanchez, and M. Antonietti, *Facile General Route toward Tunable Magnéli Nanostructures and Their Use As Thermoelectric Metal Oxide/Carbon Nanocomposites.* ACS Nano, 2011. **5**(11): p. 9052-9061.
42. Spinelli, A., M.A. Torija, C. Liu, C. Jan, and C. Leighton, *Electronic transport in doped $SrTiO_3$: Conduction mechanisms and potential applications.* Phys. Rev. B, 2010. **81**(15): p. 155110.
43. Liu, J., C.L. Wang, W.B. Su, H.C. Wang, P. Zheng, J.C. Li, J.L. Zhang, and L.M. Mei, *Enhancement of thermoelectric efficiency in oxygen-deficient $Sr_{1-x}La_xTiO_{3-\delta}$ ceramics.* Applied Physics Letters, 2009. **95**(16): p. 162110.
44. Lyeo, H.-K. and D.G. Cahill, *Thermal conductance of interfaces between highly dissimilar materials.* Phys. Rev. B, 2006. **73**(14): p. 144301.
45. Duran, A., F. Morales, L. Fuentes, and J.M. Siqueiros, *Specific heat anomalies at 37, 105 and 455 K in $SrTiO_3$: Pr.* Journal of Physics-Condensed Matter, 2008. **20**(8).
46. Traylor, J.G., H.G. Smith, R.M. Nicklow, and M.K. Wilkinson, *Lattice Dynamics of Rutile.* Phys. Rev. B, 1971. **3**(10): p. 3457-3472.

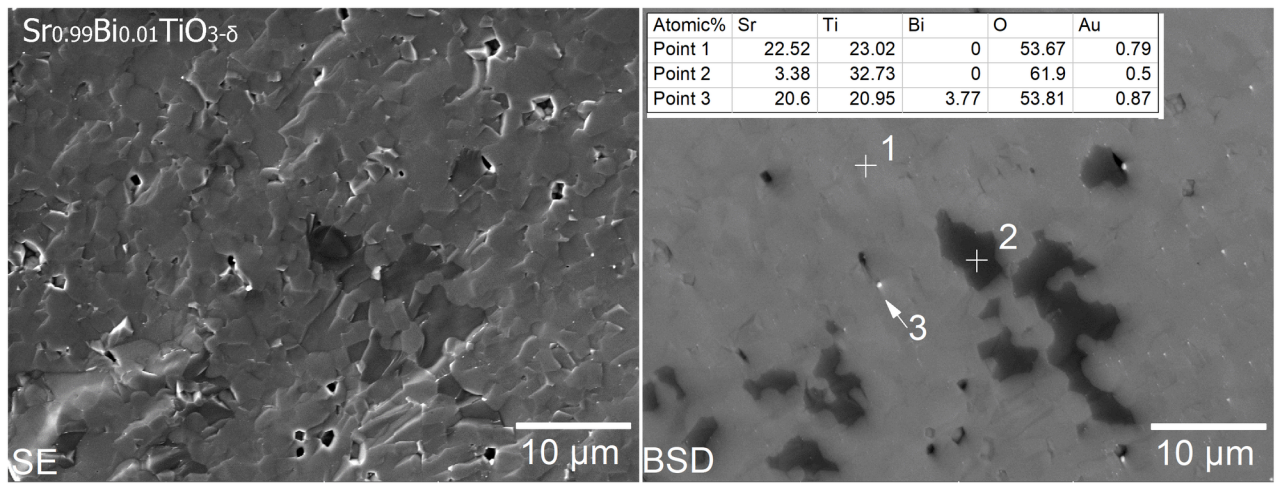

Atomic%	Sr	Ti	Bi	O	Au
Point 1	22.52	23.02	0	53.67	0.79
Point 2	3.38	32.73	0	61.9	0.5
Point 3	20.6	20.95	3.77	53.81	0.87